**Bulletin of Mathematical Biology manuscript No.**
(will be inserted by the editor)

# Population Model of Quorum Sensing With Multiple Parallel Pathways

**Gaoyang Fan**[1] **and Paul C. Bressloff**[1]

Department of Mathematics, University of Utah, Salt Lake City, UT 84112 USA

The date of receipt and acceptance will be inserted by the editor

**Abstract** Quorum sensing (QS) is a bacterial communication mechanism that uses signal-receptor binding to regulate gene expression based on cell density, resulting in group behaviors such as biofilm formation, bioluminescence and stress response. In certain bacterial species such as *V. harveyi*, several parallel QS signaling pathways drive a single phosphorylation-dephosphorylation cycle (PdPC), which in turn regulates QS target genes. In this paper, we investigate the possible role of parallel signaling pathways by developing a mathematical model of QS in *V. harveyi* at both the single-cell and population levels. First we explore how signal integration may be achieved at the single-cell level, and how different model parameters influence the process. We then consider two examples of signal integration at the population level: a one-population model responding to two environmental cues (cell density and mass transfer), and a two population model with distinct cell densities. In each case, we use contraction analysis to reduce the population model to an effective single-cell model.

**Key words** quorum sensing, phosphorylation

## 1 Introduction

Bacterial quorum sensing is a form of cellular communication mediated by extracellular signaling molecules known as *autoinducers*. Quorum sensing allows populations of bacteria to track their cell density and possibly other environmental factors, and use this as a basis for synchronizing gene expression at the population level. Many species of bacteria use quorum sensing to coordinate various types of behavior including bioluminescence, biofilm formation, virulence, and antibiotic resistance [6,3,5,13,26,24,9,17,28,16,

18]. At the single-cell level, bacteria produce autoinducers that are secreted into the extracellular environment. Each cell also has receptors that can specifically detect the signaling molecule via ligand-receptor binding, which then activates transcription of certain genes, including those for autoinducer synthesis. The probability of signal detection will depend on the local extracellular concentration of autoinducers, which itself will depend on cell density. Hence, higher cell densities will tend to generate higher concentrations of autoinducer, and thus increase the likelihood of binding to receptors and the activation of downstream gene networks.

Chemical signaling pathways often serve to amplify the sensitivity of a cell to changes in extracellular autoinducer concentration, resulting in switch-like behavior. At least two distinct mechanisms for a biochemical switch have been identified. The first is based on positive feedback in a gene regulatory network that synthesizes autoinducer, which on release into the extracellular domain can trigger activation of the same genes. Increasing the autoinducer concentration sweeps the quorum sensing network from a monostable low activity state to a monostable high activity state via a bistable regime [4]. Such a mechanism is thought to occur in the bacterium *Pseudomonas aeruginosa*, which is a human pathogen that monitors its cell density in order to control the release of various virulence factors [3,5]. An alternative, feedforward switching mechanism arises in the bacterial species *V. harveyi* and *V. cholerae* [13,24,28]. In these quorum sensing systems two or more parallel signaling pathways control a gene regulatory network via a cascade of phosphorylation-dephosphorylation cycles (PdPCs). When the proteins of the PdPCs are phosphorylated (dephosphorylated) they suppress (activate) downstream gene regulatory networks. Interconversion of the inactivated and activated protein states is catalyzed by two enzymes, *kinases* that phosphorylate the inactivated protein and *phosphotases* that dephopshorylate the activated protein. In the quorum sensing system, the binding of an autodinducer to its cognate receptor switches the receptor from acting like a kinase to one acting like a phosphotase. Thus the PdPCs are driven by the level of autoinducer which itself depends on the cell density. One characteristic feature of a PdPC is that it exhibits *ultrasenstivity*, that is, its response to a stimulus takes the form of a relatively sharp, switch-like sigmoid function [8,7,20].

Recently, we developed a feedforward, population model of quorum sensing in *V. harveyi* [1]. For simplicity, we focused on a single phosphorylation pathway based on the Goldbeter-Koshland of PdPCs [8]. Our model consisted of a system of ordinary differential equations (ODEs) that represent the interchange of an autoinducer between the cytoplasm of $N$ cells and an extracellular domain, and the binding of intracellular autoinducer to cognate receptors within each cell. The unbound and bound receptors were treated as kinases and phosphotases, respectively, acting on a single downstream PdPC network. We ignored subsequent signaling pathways associated with gene regulation and the possible modification in the production rate of autoinducer (positive feedback). We first showed how the result-

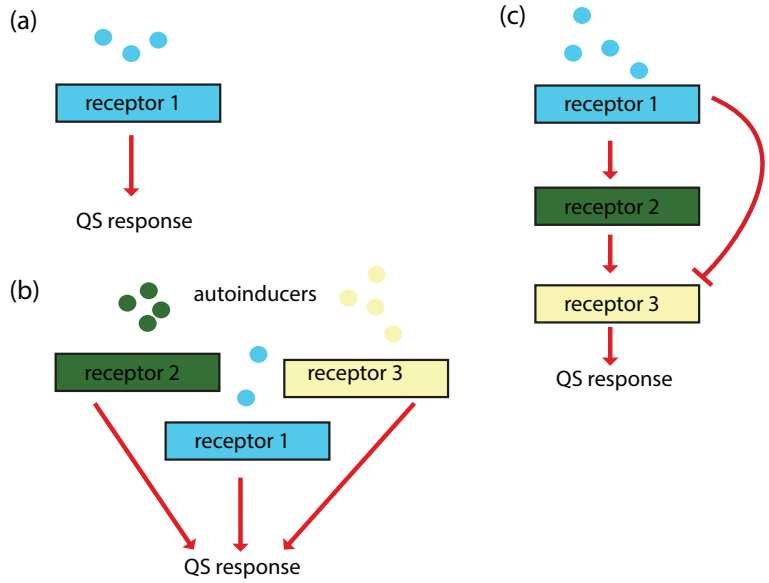



**Fig. 1** Different quorum sensing (QS) architectures. (a) One-to-one system: a single type of autoinducer (AI) and cognate receptor controls the QS response. (b) Many-to-one parallel: Information from multiple types of AI and their cognate receptors is integrated in parallel to determine the QS response. In the case of *V. harveyi* there are three distinct autoinducers (AI-1, AI-2 and CAI-1) each with a corresponding cognate receptor (LuxN, LuxP/Q, CqS), and an associated enzyme (LuxM, LuxS, CqsA) that helps produce the autoinducer. (c) Many-to-one hierarchical: Multiple receptors form a signaling cascade in which the activity of a downstream receptor is controlled by upstream receptors.

ing quorum sensing system exhibits ultrasensitivity with respect to changes in cell density, and highlighted how the resulting switch-like behavior can make the system vulnerable to fast noisy fluctuations in the environment. We then demonstrated how quorum sensing at the population level can protect against noise amplification in comparison to the PdPC of a single isolated cell.

In this paper, we extend the feedforward model of Bressloff [1] in order to study another important aspect of quorum sensing in bacteria such as *V. harveyi* and *V. cholerae*, namely the existence of several parallel autoinducer pathways [26,14,28], see Fig. 1. In particular, *V. harveyi* uses three distinct autoinducers, AI-1, AI-2 and CAI-1, each of which appears to encode distinct environmental information. (The human pathogen *V. cholerae* has up to four parallel pathways [12].) That is, the autinducers have varying levels of bacterial species specificity [26]: AI-1 is specific to *V. harveyi* and thus acts as an intraspecies signal, CA1-1 is produced primarily by vibrios, suggesting that it is an intragenera signal, whereas A1-2 is prevalent across many different bacteria thus acting as a nonspecific interspecies signal. Al-

though many types of bacteria use several parallel autoinducer pathways, it is still not clear what environmental information each of these pathways carries and how this information is integrated to determine the quorum sensing response. In the case of *V. harveyi*, it has been observed experimentally that, at the population level, cells tightly synchronize their response to a wide range of environmental conditions (different relative fractions of the three types of autoinducer), and that the signals from at least two of the autoinducers (A1-1 and AI-2) are combined strictly additively within the shared PdPC pathway [14]. Assuming that a growing population of cells varies in its level of diversity, it has been suggested that the use of multiple autoinducers allows the population to synchronize gene expression over a sequence of distinct developmental stages [14]. The additive nature of the response also suggests that the *V. harveyi* quorum sensing system operates in a graded-like rather than a switch-like manner. As far as we are aware, the nature and role of parallel pathways have not been modeled explicitly at the population level. Previous work has tended to focus on single–cell models, and to use information theoretic approaches [15]. Here we develop a population model and uses dynamical systems theoory.

The structure of the paper is as follows. In section 2, we study the "many-to-one" circuitry by constructing a single-cell model containing parallel signal-receptor binding and the receptor-driven PdPC. Treating different autoinducer concentrations as the system inputs allows us to analyze how different parameters contribute to the signal integration. Moreover, we show that the model exhibits additive response properties consistent with the experimental findings of Long et al. [14]. In section 3, we formulate a population model, in which the intracellular autodinducer concentration within each cell is no longer fixed, but is determined dynamically via the diffusive exchange of internally produced autoinducer molecules with the extracellular environment. This allows the QS response to now depend on environmental factors such as cell density. We then consider two examples of signal integration at the population level, under the assumption that the autoinducer production rates are independent of the level of quorum sensing expression (no feedback). First, in section 4, we analyze a one-population model responding to two environmental cues given by cell density and mass transfer. We also discuss the current debate between classical QS and the alternative diffusion sensing (DS) hypothesis. Second, in section 5, we analyze a two population model and determine the QS response as a function of the two distinct cell densities. In both examples, we use contraction analysis [23, 22, 1] to reduce the population model to an effective single-cell model.

## 2 Single-cell model

As we mentioned in the introduction, the bioluminescent bacterium *V. harveyi* has three parallel QS systems, each consisting of a distinct autoinducer (AI-1, AI-2, CAI-1), and a corresponding cognate receptor (LuxN,

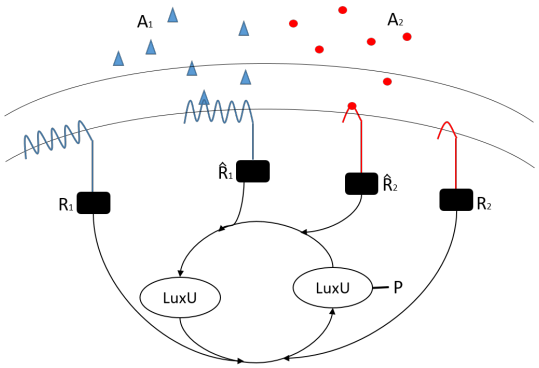



**Fig. 2** Quorum sensing circuit with two parallel pathways feeding into a LuxU phosphorylation-dephosphorylation cycle.

LuxPQ, CqsS). Consider for the moment a single cell subject to some fixed background concentration of a single autoinducer. At low autoinducer concentrations there is a low probability that an autoinducer ligand can bind to its cognate receptor. Consequently, the receptor acts as a kinase that autophosphorylates, and subsequently transfers its phosphate to a cytoplasmic protein known as LuxU to form LuxU-P. The latter then passes its phosphate to the DNA-binding regulatory protein LuxO to yield LuxO-P. At low autoinducer concentrations, the ratio of [LuxO-P] to [LuxO] is high and this activates transcription of the genes encoding five regulatory small non-coding RNAs (sRNAs) termed Qrr1-Qrr5 (Quorum Regulatory RNA). Qrr1–Qrr5 destabilize the transcriptional activator protein LuxR, thus preventing the activation of target genes responsible for the production of various proteins, including bioluminescent luciferase. On the other hand, at higher autoinducer concentrations, there is a higher probability of binding to a receptor, which then switches from a kinase to a phosphotase, significantly reducing the ratio of [LuxO-P] to [LuxO]. The sRNAs are thus no longer expressed, allowing the synthesis of LuxR and the expression of bioluminescence, for example. Both the phosphorylation-dephosphorylation cascades [1] and the sRNA regulatory network [11] provide a basis for a sigmoidal-like response of the concentration of LuxR to smooth changes in cell density.

In this section, we consider an extension of the single-cell model introduced by Bressloff [1], by considering multiple autoinducer signaling pathways feeding into a single PdPC, see Fig. 2. In particular, we consider the phosphorylation-dephosphorylation of LuxU by the enzymatic action of several types of QS receptor, which are denoted by $R_i$ when acting as a kinase and by $\widehat{R}_i$ when bound by the corresponding autoinducer type ($A_i$) and acting like a phosphotase. Let $W$ denote protein LuxU and $W^*$ denote LuxU-P. By the Goldbeter-Koshland model of PdPCs [8], QS with $M$ parallel path-

way can be represented by the following reaction scheme:

$$W + R_i \underset{d_i}{\overset{a_i}{\rightleftharpoons}} WR_i \xrightarrow{g_i} W^* + R_i, \tag{2.1a}$$

$$R_i + A_i \underset{k_{-i}}{\overset{k_i}{\rightleftharpoons}} \hat{R}_i, \tag{2.1b}$$

$$W^* + \hat{R}_i \underset{c_i}{\overset{b_i}{\rightleftharpoons}} W^*\hat{R}_i \xrightarrow{h_i} W + \hat{R}_i. \tag{2.1c}$$

To write down the governing differential equations, let $[W] = w$, $[W^*] = w^*$, $[R_i] = r_i$, $[\hat{R}_i] = \hat{r}_i$, $[WR_i] = v_i$, $[W^*R_i] = v_i^*$ and $[A_i] = u_i$. By the law of mass action, the kinetic equations for a single cell with fixed intracellular concentration of inducers $u_i$ are:

$$\dot{w} = \sum_{i=1}^{M} -a_i(r_i - v_i)w + d_i v_i + h_i v_i^*, \tag{2.2a}$$

$$\dot{v}_i = a_i(r_i - v_i)w - (d_i + g_i)v_i, \tag{2.2b}$$

$$\dot{w}^* = \sum_{i=1}^{M} -b_i(\hat{r}_i - v_i^*)w^* + c_i v_i^* + g_i v_i, \tag{2.2c}$$

$$\dot{v}_i^* = b_i(\hat{r}_i - v_i^*)w^* - (c_i + h_i)v_i^*, \tag{2.2d}$$

$$\dot{r}_i = k_{-i}\hat{r}_i - k_i r_i u_i. \tag{2.2e}$$

By the conservation law for protein LuxU and receptors, system (2.2) is constrained by the following conditions:

$$W_T = w + w^* + \sum_{i=1}^{M}(v_i + v_i^*), \tag{2.3a}$$

$$R_{Ti} = r_i + \hat{r}_i, \tag{2.3b}$$

where $W_T$ represents the total concentration of protein LuxU and $R_{Ti}$ represents the total concentration of the receptor $i$.

In this single-cell model, we treat the concentration of the inducers $A_i$ as the external input, which leads to the decoupling of equation (2.2e) from the remaining equations system (2.2a-d). For a fixed value of $u_i$, we see that $r_i$ has a stable equilibrium at

$$r_i^{eq} = \frac{k_{-i}}{k_{-i} + k_i u_i} R_{Ti} \equiv G_i(u_i), \tag{2.4a}$$

$$\hat{r}_i^{eq} = R_{Ti} - G_i(u_i). \tag{2.4b}$$

Further, we assume that the concentration of LuxU is much larger than the concentration of the receptors, which implies that $W_T \approx w + w^*$. Since the time scale of the dynamics of the product concentrations $v_i$ and $v_i^*$ tends

to be much faster than the time scale for $w$ and $w^*$, it follows that the fast dynamics quickly approaches its stable equilibrium at

$$v_i^{eq} = \frac{a_i w}{a_i w + d_i + g_i} r_i^{eq}, \tag{2.5a}$$

$$v_i^{*eq} = \frac{b_i w^*}{a_i w^* + c_i + h_i} \hat{r}_i^{eq}. \tag{2.5b}$$

Under this adiabatic approximation, the slow system can be simplified as the following scheme:

$$W \underset{f_2(w^*,\mathbf{u})}{\overset{f_1(w,\mathbf{u})}{\rightleftharpoons}} W^*. \tag{2.6}$$

By the conservation law of $W_T = w + w^*$, the system can be further reduced to the following kinetic equation:

$$\dot{w}^* = f_1(W_T - w^*, \mathbf{u}) - f_2(w^*, \mathbf{u}) \equiv f(w^*, \mathbf{u}), \tag{2.7}$$

where $\mathbf{u} = (u_1, \ldots, u_M)^\top$,

$$f(w^*, \mathbf{u}) = \sum_{i=1}^{M} \left[ \frac{g_i G_i(u_i)(W_T - w^*)}{W_T - w^* + K_i} - \frac{h_i [R_{Ti} - G_i(u_i)] w^*}{w^* + Q_i} \right], \tag{2.8}$$

and

$$K_i = \frac{d_i + g_i}{a_i}; \quad Q_i = \frac{c_i + h_i}{b_i}. \tag{2.9}$$

To reduce the dimension of the parameter space, we will apply nondimensionalization on system (2.7). Let $\phi$ and $\tau$ denote nondimensionalized Lux-P concentration and time, respectively:

$$\phi = \frac{w^*}{W_T}; \quad \tau = \frac{g_1 R_{T1}}{W_T} t. \tag{2.10}$$

To simplify the calculation, we assume that $K = K_i/W_T$ and $Q = Q_i/W_T$ for all $i = 1, \ldots, M$. After some algebra, one can show that,

$$\frac{d\phi}{d\tau} = \frac{A(\mathbf{u})\phi^2 - B(\mathbf{u})\phi + C(\mathbf{u})}{(\phi + Q)(1 + K - \phi)}, \tag{2.11}$$

where

$$A(\mathbf{u}) = \sum_{i=1}^{M} \Lambda_i \frac{\beta_i \alpha_i u_i - 1}{1 + \alpha_i u_i}, \tag{2.12a}$$

$$C(\mathbf{u}) = \sum_{i=1}^{M} \Lambda_i \frac{Q}{1 + \alpha_i u_i}, \tag{2.12b}$$

$$B(\mathbf{u}) = (1 + K)A(\mathbf{u}) + (1 + K/Q)C(\mathbf{u}), \tag{2.12c}$$

and

$$\alpha_i = \frac{k_i}{k_{-i}}, \quad \beta_i = \frac{h_i}{g_i}, \quad \Lambda_i = \frac{R_{Ti}}{R_{T1}} \frac{g_i}{g_1}. \tag{2.13}$$

To find the steady state of $\phi$ as a function of the vector $\mathbf{u}$ of autoinducer concentrations, we simply need to solve the quadratic $A(\mathbf{u})\phi^2 + B(\mathbf{u})\phi + C(\mathbf{u}) = 0$ on the domain $[0,1]$, which gives

$$\phi^{eq}(\mathbf{u}) = \begin{cases} \dfrac{B(\mathbf{u}) - \sqrt{B(\mathbf{u})^2 - 4A(\mathbf{u})C(\mathbf{u})}}{2A(\mathbf{u})}; & A(\mathbf{u}) \neq 0 \\ \dfrac{Q}{Q+K}; & A(\mathbf{u}) = 0. \end{cases} \tag{2.14}$$

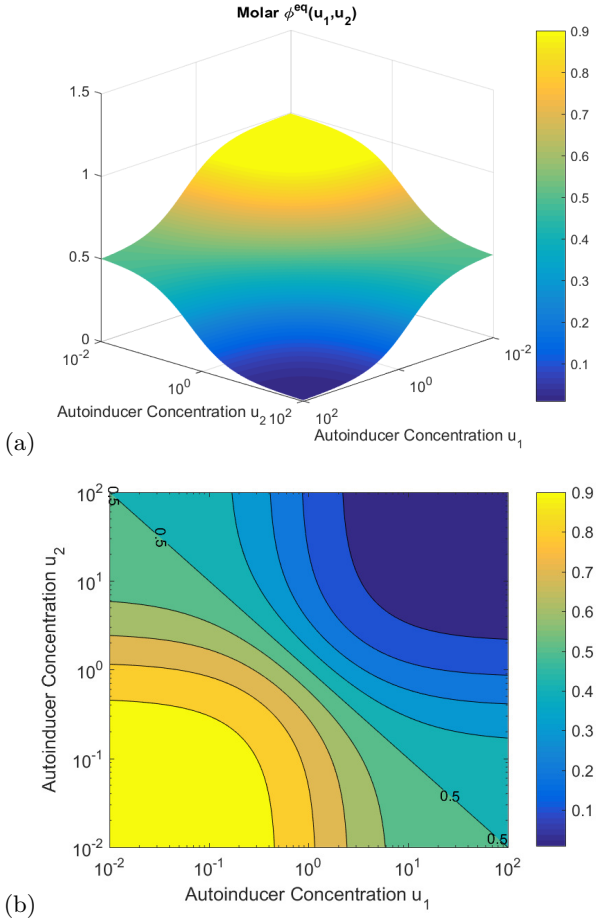



**Fig. 3** LuxU-P Response curve to autoinducer inputs (a) 3D plot of $\phi^{\rm eq}(u_1, u_2)$. (b) Corresponding contour plot. Dark blue represents QS being ON and light yellow represents QS being OFF. Parameters values are as follows: $\alpha_1 = \alpha_2 = 1$, $\beta_1 = \beta_2 = 1$, $\Lambda_1 = \Lambda_2 = 1$ and $K = Q = 1$.

Linearizing system (2.11) about the steady state $\phi^{eq} \in [0,1]$, we find that $\dot{\phi} = D\phi$, where

$$D = \begin{cases} -\dfrac{\sqrt{B^2 - 4AC}}{(\phi^{eq}+Q)(1+K-\phi^{eq})}; & A \neq 0 \\ \\ -\dfrac{C}{(\phi^{eq}+Q)(1+K-\phi^{eq})}; & A = 0. \end{cases} \tag{2.15}$$

One can show that $D < 0$, which indicates that $\phi^{eq}$ is a stable equilibrium.

To demonstrate how PdPC response to different combinations of autoinducer signal inputs and the roles of different parameters in the system, we graphed the Lux-P concentration $\phi^{eq}$ as a function of autoinducer concentrations $u_i, i = 1, \ldots, M$ for the case $M = 2$, see Fig. 3. It can be seen that low (high) autoinducer concentrations lead to high (low) LuxU-P concentrations, which matches the case $M = 1$ [1]. Since LuxU-P acts like a repressor in the QS system, it follows that low autoinducer concentrations turn the QS response OFF while high autoinducer concentrations turn the QS response ON. Another feature of the response is that it is symmetric with respect to $u_1$ and $u_2$, which is a consequence of the fact that we have taken all parameters of the two autoinducer pathways to be identical. One consequence of this symmetry is that the system cannot distinguish between the two states High A1/Low A2 and Low A1/High A2. That is, assuming that the response is graded rather than switch-like, then the system can roughly distinguish between three regimes: Low A1/Low A2 (small response), High A1/High A2 (large response) and the mixed High/Low state (intermediate response), see Fig. 3. The inability to distinguish High/Low from Low/High

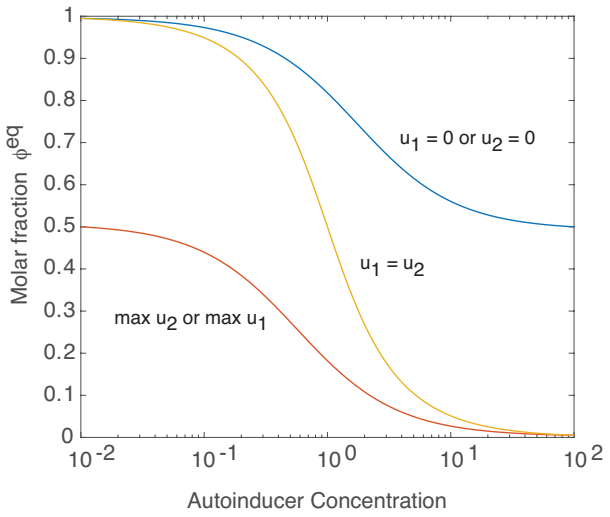



**Fig. 4** Quorum sensing response to different combination of autoinducer inputs. The parameters are the same as Fig. 3

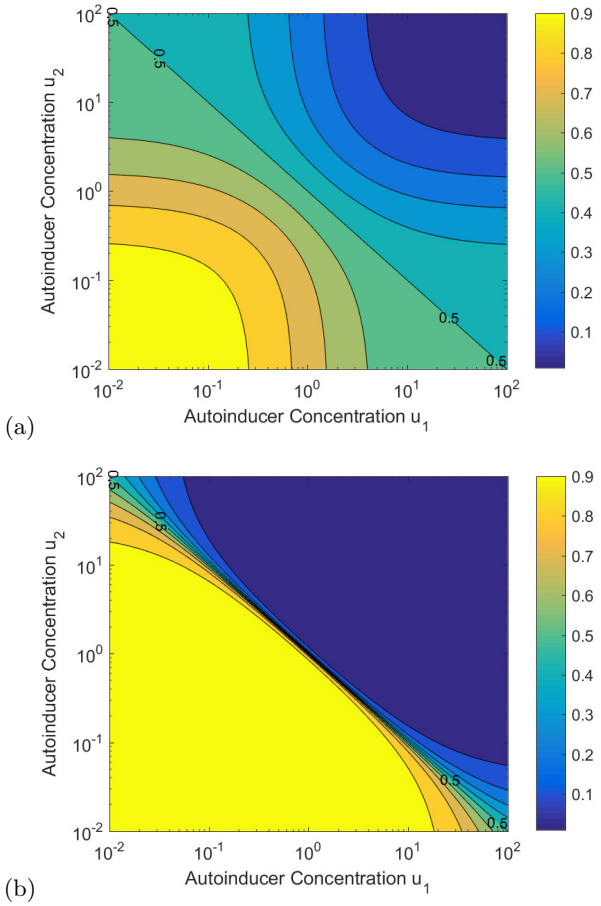



**Fig. 5** PdPC response for different value of $K$ and $Q$ for $K = Q$. Contour plots of $\phi^{\rm eq}(u_1, u_2)$ for (a) $K = Q = 10$ and (b) $K = Q = 0.01$, respectively. All other parameters are the same as Fig. 3.

might be mitigated if different autoinducers are prevalent at different stages of development [14]. Another way to interpret the response properties of the PdPC is that the system effectively acts like a fuzzy version of an AND gate, since it only exhibits a large response when both input channels are high.

Our single-cell model matches experimental data on the additive nature of the response of *V. harveyi* to the pair of autoinducers AI-1 and AI-2 [14]. Long et al. [14] created three different bacterial strains. The LuxN$^+$ strain carried wild-type luxN on the chromosome and was deleted for cqsS and luxPQ. Hence, only the A1 receptors were present in the mutant. The strain was also deleted for luxM, encoding the AI-1 synthase LuxM, and was therefore exclusively responsive to exogenously added AI-1. (In our model this corresponds to fixing $u_1$ and setting $u_2 = 0$). On the other hand, the

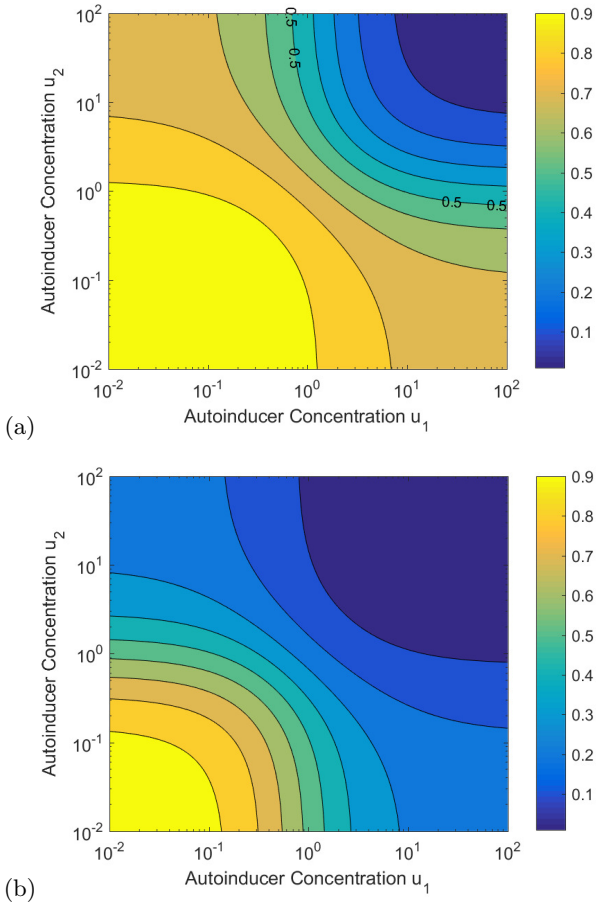



**Fig. 6** PdPC response for different value of $K$ and $Q$ for $K \neq Q$. Contour plots of $\phi^{\text{eq}}(u_1, u_2)$ for (a) $K = 1$, $Q = 3$ and (b) $K = 3$, $Q = 1$, respectively. All other parameters are the same as Fig. 3.

LuxPQ+ strain was deleted for luxN and cqsS as well as luxS encoding the AI-2 synthase. Hence, this strain was only responsive to exogenous AI-2 (corresponding to setting $u_1 = 0$ and fixing $u_2$ in our model). Finally, the combined LuxN$^+$LuxPQ$^+$ strain lacked cqsS, luxM, and luxS, and was thus responsive to exogenously supplied AI-1 and AI-2. (Fixed $u_1, u_2$). The response of these mutants to external auotonducer concentrations was measured by fusing gfp to the qrr4 promoter, which is one of the genes encoding the quorum-sensing sRNAs that are activated by LuxO-P. Thus the level of GFP indicated the level of suppression of the target genes, and is analogous to the equilibrium molar fraction $\phi^{eq}$ in our model. Similar to Long et al, we tested the response curves under three different scenarios: response to equal amounts of both autoinducer, and response to one of the autoinducer

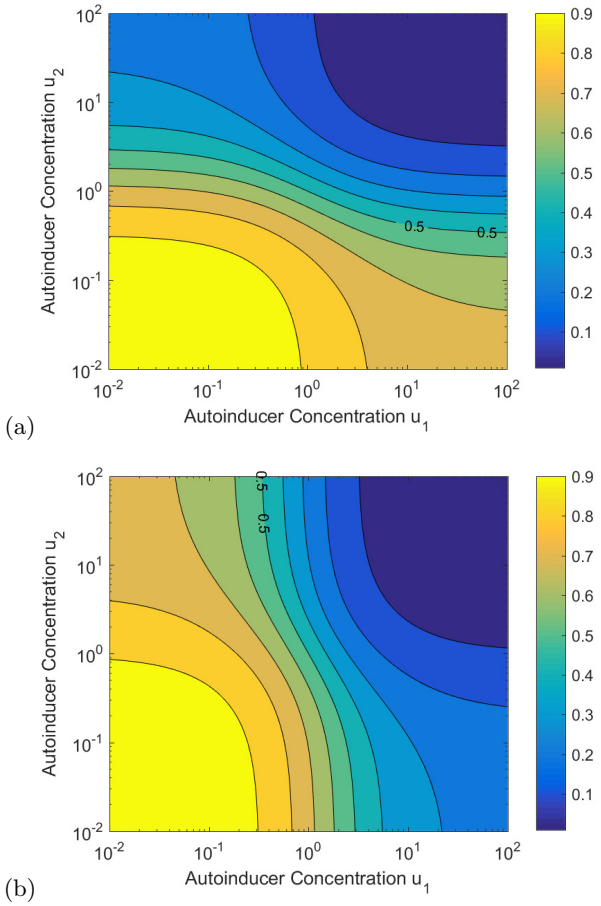



**Fig. 7** Signal discrimination in quorum sensing due to different receptor numbers. Contour plots of $\phi^{\rm eq}(u_1, u_2)$ for (a) $\Lambda_2 = 2$ (b) $\Lambda_2 = 0.5$. All other parameters are the same as Fig. 5.

input with either no input from the other autoinducer or maximum input from the other autoinducer. The results are shown in Fig. 4, and match very well the experimental results shown in Fig. 3B of [14].

The response to changes in the autoinducer concentrations becomes more switch-like as we decrease the value of $K$ and $Q$. This is illustrated in Fig. 5 (where $K = Q$. Recall that $K$ is the ratio of $(d_i + g_i)/a_i$. As $K$ decreases, $a_i$ becomes relatively large, which implies that the unbounded receptor will quickly phosphorylate LuxU. Similarly, $Q$ is the ratio $(c_i + h_i)/b_i$ so that as $Q$ increases, the bounded receptor will quickly dephosphorylate LuxU-P. Either way, efficient phosphorylation or dephosphorylation results in a more switch-like response. On the other hand, if we set $K$ and $Q$ to be different values, as shown in Fig. 6, we observe a shift of the contour

lines. So far we have assumed that the response is symmetric with respect to the two autoinducers. One possible mechanism for breaking this symmetry would be differences in the total amount of receptors $R_{Ti}$ for $i = 1, 2$. This is illustrated in Fig. 7, where we plot the response $\phi^{eq}$ for different values of the dimensionless parameter $\Lambda_2 = R_{T2}/R_{T1}$ (assuming $g_1 = g_2$). By comparing the contour plots with the symmetric case in Fig. 3(b), we see that the level curves are more horizontal (vertical) when $\lambda_2 = 2$ (when $\Lambda_2 = 0.5$), which means that the response is more biased towards signal $A_2$ (signal $A_1$). The appearance of such vertical and horizontal contours are also observed in experiments [25].

## 3 Population model

We now consider a population model with $N$ identical cells ($j = 1, \ldots, N$), each producing/detecting $M$ types of autoinducer ($i = 1, \ldots, M$), see Fig. 8. The cells are coupled via a common extracellular domain due to the transfer of the autoinducer $A_i$ across the cell membrane. Eq. (2.2e) for a single cell is then replaced by a system of equations of the form

$$\dot{r}_{ij} = k_{-i}(R_{Ti} - r_{ij}) - k_i r_{ij} u_{ij}, \tag{3.1a}$$

$$\dot{u}_{ij} = \Gamma_i + k_{-i}(R_{Ti} - r_{ij}) - k_i r_{ij} u_{ij} - \kappa_i(u_{ij} - U_i), \tag{3.1b}$$

$$\dot{U}_i = \rho\kappa_i(u^i_{av} - U_i) - \gamma_i U_i, \tag{3.1c}$$

for $i = 1, \ldots, M$, $j = 1, \ldots, N$ with

$$u^i_{av} = \frac{1}{N}\sum_{j=1}^{N} u_{ij}. \tag{3.2}$$

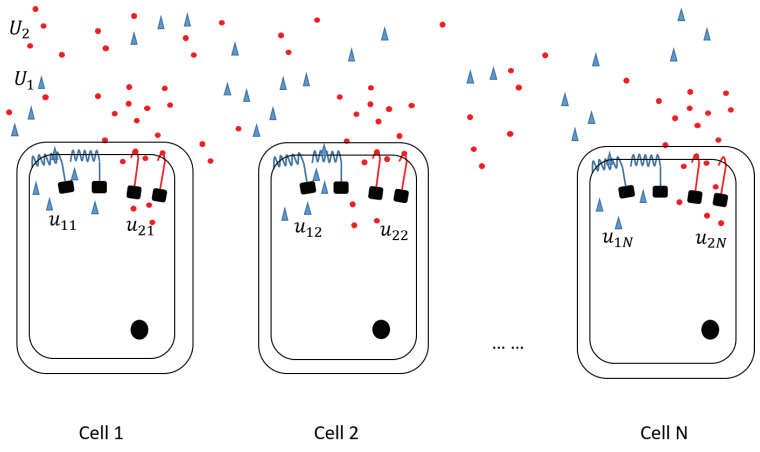



**Fig. 8** $N$ identical cells with two different types of autoinducers ($M = 2$).

Here $U_i$ represents the concentration of autoinducer $A_i$ in the extracellular domain while $u_{ij}$ represents the concentration of autoinducer $A_i$ inside cell $j$. Moreover, the term $\kappa_i(u_{ij}-U_i)$ represents the diffusive exchange of signaling molecules $A_i$ across the membrane of the jth cell with diffusive conductance $\kappa_i$, $\Gamma_i$ represents the fixed production rate of the signaling molecule $A_i$ with decay rate $\gamma_i$. Finally, the extracellular environment is represented by the parameter $\rho = Nv_{cyt}/V_{ext}$. This represents the cell density in terms of the ratio of total cytosolic volume and the extracellular volume.

In the absence of any feedback loops, the dynamics of the different autoinducers are decoupled. Therefore, we can extend the single-channel analysis of Bressloff [1], to prove that under wide range of parameter values, the solution of equations (3.1) will converge globally to the solution of an effective single-cell model. Since the analysis is similar to the single-channel case, we only sketch the basic steps here and refer the reader to Ref. [1] for more details. The basis of the proof is so-called contraction analysis [22].

The first step is to consider a single autoinducer by fixing $i$, and rewriting equations (3.1a,b) in the form

$$\frac{d\mathbf{x}_j^i}{dt} = \mathbf{F}^i(\mathbf{x}_j^i,t) \equiv \mathbf{f}^i(\mathbf{x}_j^i,t) + \Gamma_i \begin{pmatrix} 1 \\ 0 \end{pmatrix}, \quad j = 1,\ldots,N \tag{3.3}$$

with $\mathbf{x}_j^i = (u_{ij}, r_{ij}) \in \mathbb{R}^2$, $(\mathbf{x}_j^i)_1 = u_{ij}$, and

$$f_1^i(\mathbf{y},t) = k_{-i}(R_{Ti} - y_2) - k_i y_1 y_2 - \kappa_i(y_1 - U_i(t)) \tag{3.4a}$$

$$f_2^i(\mathbf{y},t) = k_{-i}(R_{Ti} - y_2) - k_i y_1 y_2. \tag{3.4b}$$

Note that here the extracellular concentration $U_i(t)$ for fixed $i$ is treated as a common time-dependent input. In order to apply contraction analysis, we will specify the basic contraction theorem in terms of a non-autonomous dynamical system on $\mathbb{R}^n$, and then set $n = 2$. In order to proceed we need to introduce a norm on any vector $\mathbf{y} \in \mathbb{R}^n$ and specify the induced matrix norm for an arbitrary $n \times n$ square matrix $\mathcal{A}$, that is,

$$\|A\| = \sup\{|A\mathbf{y}| : \mathbf{y} \in \mathbb{R}^n \text{ with } |\mathbf{y}| = 1\}.$$

For concreteness, we choose the $\ell_2$ norm so that

$$|\mathbf{y}|_2 = \left( \sum_{k=1}^n |y_k|^2 \right)^{1/2}, \quad \|A\|_2 = \sqrt{\lambda_{\max}(A^*A)},$$

where $A^*$ is the transpose of $A$ and $\lambda_{\max}(A^*A)$ is the largest eigenvalue of the positive semi-definite matrix $A^*A$. Define the associated matrix measure $\mu$ as

$$\mu(A) = \lim_{h \to 0^+} \frac{1}{h}(\|I + hA\| - 1),$$

where $I$ is the identity matrix. For the $\ell_2$ norm on $\mathbb{R}^n$, the associated matrix measure is

$$\mu_2(A) = \max_{1\leq k\leq n} \{\lambda_k([A + A^*]/2)\}.$$

Given these definitions, the basic contraction theorem is as follows [22]:

**Theorem 1** *An $n$-dimensional dynamical system $\dot{\mathbf{y}} = \mathbf{F}(\mathbf{y}, t)$ is said to be contracting if any two trajectories, starting from different initial conditions, converge exponentially to each other. A sufficient condition for a system to be contracting is the existence of some matrix measure $\mu$ for which there exists a constant $\eta > 0$ such that*

$$\mu(J(\mathbf{x}, t)) \leq -\eta, \quad J_{kl} = \frac{\partial F_k}{\partial y_l} \tag{3.5}$$

*for all $\mathbf{y}, t$. The scalar $\lambda$ defines the rate of contraction.*

In order to apply the contraction theorem to equation (3.3) we set $n = 2$ and consider the so-called virtual system

$$\frac{d\mathbf{y}}{dt} = \mathbf{f}^i(\mathbf{y}, t) + \Gamma_i \begin{pmatrix} 1 \\ 0 \end{pmatrix} \tag{3.6}$$

for fixed $i$. The Jacobian of the virtual system is

$$J_i(\mathbf{y}, t) = \begin{pmatrix} -k_i y_2 - \kappa_i & -k_{-i} - k_i y_1 \\ -k_i y_2 & -k_{-i} - k_i y_1 \end{pmatrix}. \tag{3.7}$$

Suppose that we take the $\ell_2$ norm for $\mathbf{y}$. In order to determine the corresponding matrix measure $\mu_2(J_i)$, we need to calculate the eigenvalues of the symmetric matrix

$$\frac{J_i + J_i^*}{2} = \begin{pmatrix} -k_i y_2 - \kappa_i & -[k_{-i} + k_i(y_1 + y_2)]/2 \\ -[k_{-i} + k_i(y_1 + y_2)]/2 & -k_{-i} - k_i y_1 \end{pmatrix}.$$

These are given by

$$\lambda_\pm^i = \frac{1}{2}\left[-b_i(\mathbf{y}) \pm \sqrt{b_i(\mathbf{y})^2 - c_i(\mathbf{y})}\right],$$

with

$$b_i(\mathbf{y}) = \kappa_i + k_{-i} + k_i(y_1 + y_2),$$
$$c_i(\mathbf{y}) = 4(\kappa_i + k_i y_2)(k_{-i} + k_+ y_1) - [k_{-i} + k_i(y_1 + y_2)]^2.$$

Since $b_i(\mathbf{y}) > 0$, the matrix measure is

$$\mu_2(J_i) = \max\{\lambda_\pm^i\} = \lambda_+^i.$$

Hence, the virtual system is contracting provided that $c_i(\mathbf{y}) > 0$. Proceeding along identical lines to Ref. [1], it can be proven that $c_i(\mathbf{y})$ is positive definite provided that the following conditions hold:

$$k_i R_{Ti} < k_{-i} < 4\kappa_i, \tag{3.8}$$

and

$$k_{-i} + k_i \Theta_i < 2\kappa_i, \quad \Theta_i \equiv \frac{(\Gamma_i + k_{-i} R_{Ti})(\alpha_i \kappa_i + \gamma_i)}{\kappa_i \gamma_i}. \tag{3.9}$$

In conclusion, if conditions (3.8) and (3.9) hold for a given $i$, then $\mu_2(J_i) < 0$ and the $\mathbf{y}$ dynamics in equation (3.6) is contracting. Setting $\mathbf{y}(t) = \mathbf{x}_j^i(t)$ in the virtual system then recovers the dynamics of $A_i$ for the $j$th cell. Hence, $\mathbf{x}_j^i(t)$ for $j = 1, \ldots, N$ and fixed $i$ are particular solutions of the virtual system so that if the virtual system is contracting in $\mathbf{y}$, then all of its solutions converge exponentially toward each other, including the solutions $x_j^i(t)$. That is, $u_{ij}(t) \to u_i(t)$ and $r_{ij}(t) \to r_i(t)$ in the large time limit. Finally, if we assume the virtual system is contracting for all autoinducers $i = 1, \ldots, M$, that is, conditions (3.8) and (3.9) hold for all $i = 1, \ldots, M$, then the population model (3.1) reduces to the effective single-cell model

$$\dot{r}_i = k_{-i}(R_{Ti} - r_i) - k_i r_i u_i, \tag{3.10a}$$

$$\dot{u}_i = \Gamma_i + k_{-i}(R_{Ti} - r_i) - k_i r_i u_i - \kappa_i(u_i - U_i), \tag{3.10b}$$

$$\dot{U}_i = \rho \kappa_i (u_i - U_i) - \gamma_i U_i \tag{3.10c}$$

for $i = 1, \ldots, N$. These equations have the unique stable fixed point $\mathbf{u} = \mathbf{u}^*$ with

$$u_i^* = \frac{\Gamma_i}{\gamma_i}\rho + \frac{\Gamma_i}{\kappa_i} \equiv \psi_i(\rho). \tag{3.11}$$

Hence, setting $u_i = u_i^*$ in equation (2.14) finally shows that the steady-state fractional concentration of LuxU-P is

$$\frac{[\text{LuxU-P}]}{[\text{LuxU-P}]+[\text{LuxU}]} = \phi^{\text{eq}}(\boldsymbol{\psi}(\rho)) \equiv \Psi(\rho). \tag{3.12}$$

We now see a major simplification of the current one-population model, namely, the response of the population only depends on one environmental variable, which is the total population density $\rho$. Therefore, in order to investigate how a population responds to more than one environmental variable, we consider two extensions of system (3.1). The first is a one-population model with two environmental variables, namely, cell density and diffusion or mass transfer (see section 4), and the second is a two population model with distinct cell densities (see section 5).

## 4 One-population model with mass-transfer: QS versus DS

Although there have been several advances in identifying the cellular mechanisms underlying QS in a variety of bacterial species, there is still disagreement concerning the functional significance of QS, in particular, how QS contributes to bacterial fitness [10,21,29,19]. The classical view is that QS allows bacteria to sense and respond appropriately to different levels of bacterial population density. The main alternative is the so-called diffusion sensing (DS) hypothesis, which suggests that variation in the concentration of extracellular signaling molecules is primarily determined by physical mass transfer effects such as diffusion or advection, rather than bacterial density, see Fig. 9. One argument for DS is that in natural environmental settings, bacterial growth tends to occur at much lower densities than under laboratory conditions, so that the primary information encoded by variation in signal concentration is variation in the mass transfer properties of the local environment [21].

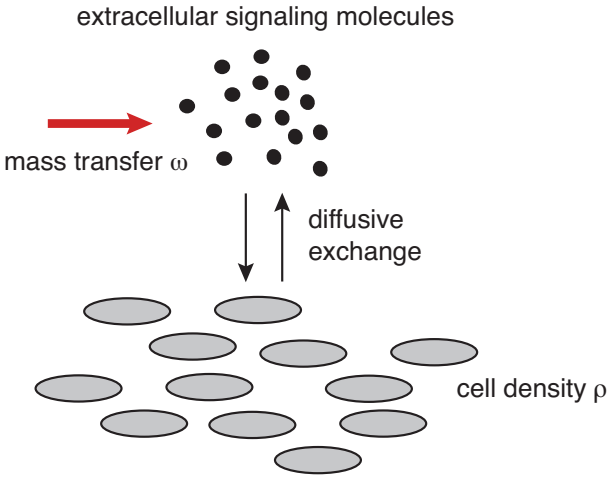



**Fig. 9** Population of bacterial cells exchanging signaling molecules with the extracellular environment in the presence of mass transfer effects. The extracellular/intracellular concentrations of the signaling molecule will depend on cell density $\rho$ and the rate of mass transfer $\omega$.

Irrespective of whether the QS or DS viewpoint is more appropriate, it is clear that the occurrence of two environmental factors, namely, cell density and mass transfer, means that determining one of these quantities by sensing an autoinducer concentration can be confounded by the presence of the other. For example, high-density, high mass transfer environments may be indistinguishable from low-density, low mass transfer environments. In certain cases this may not be a problem, particularly if the QS system

upregulates the gene expression of secretory molecules that exert direct control over the environment [10]. That is, only high extracellular signal concentrations will lead to high concentrations of costly secreted enzymes, and this will occur under the favorable combination of low mass transfer rates and high population densities. In other words, the QS system simply needs to detect the regime of high density/low mass transfer.

The above argument breaks down when targets of the QS system are non-secretory molecules such as those responsible for bioluminescence in *V. harveyi*. The effectiveness of group luminescence only depends on cell density and should not be affected by mass transfer. However, the latter can still have a substantial impact on QS molecule concentration, and thus cause cells to underestimate cell density. One possible way to mitigate the affects of mass transfer is to use more than one signaling molecule (parallel autoinducer pathways), as recently demonstrated by Cornforth et al for the pathogen *Pseudomonas aeruginosa* [2,19]. They proposed a so-called "durable-fragile" signaling scheme in which one autoinducer has a much faster decay rate than another. This means that at low mass transfer rates, the fast decaying (fragile) molecules have time to break down in the vicinity of the cells, so that the concentration of the durable autoinducer is relatively high. This affect is then masked at high mass transfers, since both types of autoinducer are swept away before the fragile molecules have had a chance to decay. The presence of two distinct autoinducers allows the system to discriminate more effectively between cell density and mass transfer.

In this section we use our one-population model of *V. harveyi* QS with two parallel pathways ($M = 2$) to explore how the bacteria integrate both social (cell density) and physical (mass-transfer) environmental information. One major difference from the studies of [2,19] is that both pathways combine into a single pathway (the PdPC) before acting on gene expression. Adding a mass-transfer term with rate $\omega$ to our one-population model (3.1) gives

$$\dot{r}_{ij} = k_{-i}(R_{Ti} - r_{ij}) - k_i r_{ij} u_{ij}, \tag{4.1a}$$

$$\dot{u}_{ij} = \Gamma_i + k_{-i}(R_{Ti} - r_{ij}) - k_i r_{ij} u_{ij} - \kappa_i(u_{ij} - U_i), \tag{4.1b}$$

$$\dot{U}_i = \rho\kappa_i(u^i_{av} - U_i) - (\gamma_i + \omega)U_i, \tag{4.1c}$$

for $i = 1, 2$, $j = 1, \ldots, N$ with

$$u^i_{av} = \frac{1}{N}\sum_{j=1}^{N} u_{ij}. \tag{4.2}$$

Applying the contraction analysis of section 3, we obtain conditions (3.8) and (3.9), with

$$\Theta_i \equiv \frac{(\Gamma_i + k_{-i}R_{Ti})(\alpha_i\kappa_i + \gamma_i + \omega)}{\kappa_i(\gamma_i + \omega)}. \tag{4.3}$$

Equations (4.1) thus reduce to the following single-cell model:

$$\dot{r}_i = k_{-i}(R_{Ti} - r_i) - k_i r_i u_i, \tag{4.4a}$$
$$\dot{u}_i = \Gamma_i + k_{-i}(R_{Ti} - r_i) - k_i r_i u_i - \kappa_i(u_i - U_i), \tag{4.4b}$$
$$\dot{U}_i = \rho\kappa_i(u_i - U_i) - (\gamma_i + \omega)U_i \tag{4.4c}$$

for $i = 1, \ldots, N$, with a unique fixed point at $\mathbf{u} = \mathbf{u}^*$:

$$u_i^* = \frac{\Gamma_i \rho}{\gamma_i + \omega} + \frac{\Gamma_i}{\kappa_i} \equiv \psi_i(\rho, \omega). \tag{4.5}$$

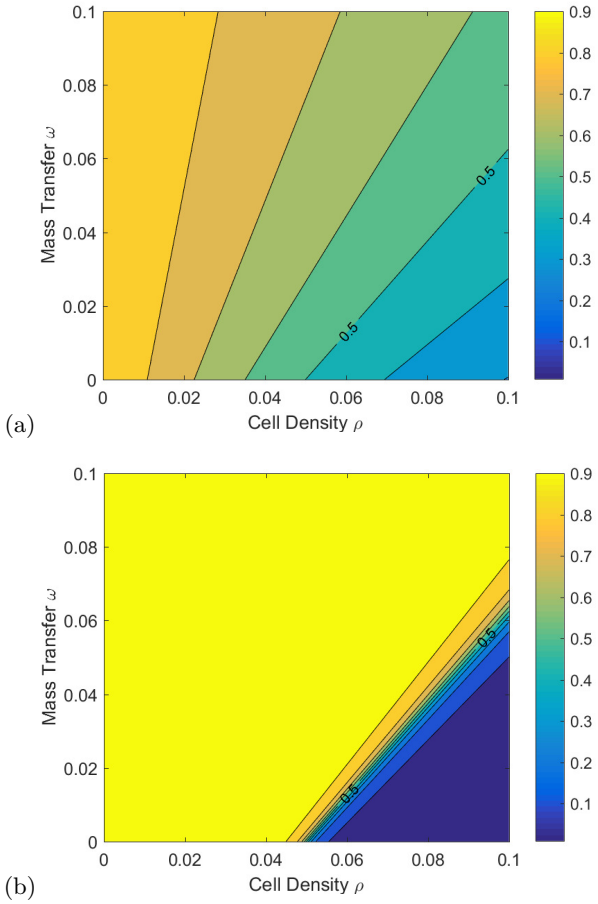



**Fig. 10** LuxU-P response to different environmental inputs in the one-population model with different response sensitivity controlled by the parameters $K$ and $Q$. Contour plots of $\Psi(\rho, \omega)$ for (a) $K = Q = 1$ and (b) $K = Q = 0.01$, respectively. Parameters used are $\Gamma_1 = \Gamma_2 = 1$, $\gamma_1 = \gamma_2 = 0.0625$, $\kappa_1 = \kappa_2 = 5$ and the rest are the same as Fig. 3.

Substituting $u_i = u_i^*$ into equation (2.14) yields

$$\frac{[\text{LuxU-P}]}{[\text{LuxU-P}]+[\text{LuxU}]} = \phi^{\text{eq}}\left(\boldsymbol{\psi}(\rho,\omega)\right) \equiv \Psi(\rho,\omega). \tag{4.6}$$

Equation (4.6) determines the PdPC response to the environmental variables $(\rho,\omega)$, see Fig. 10. In particular, we see that the QS system is only

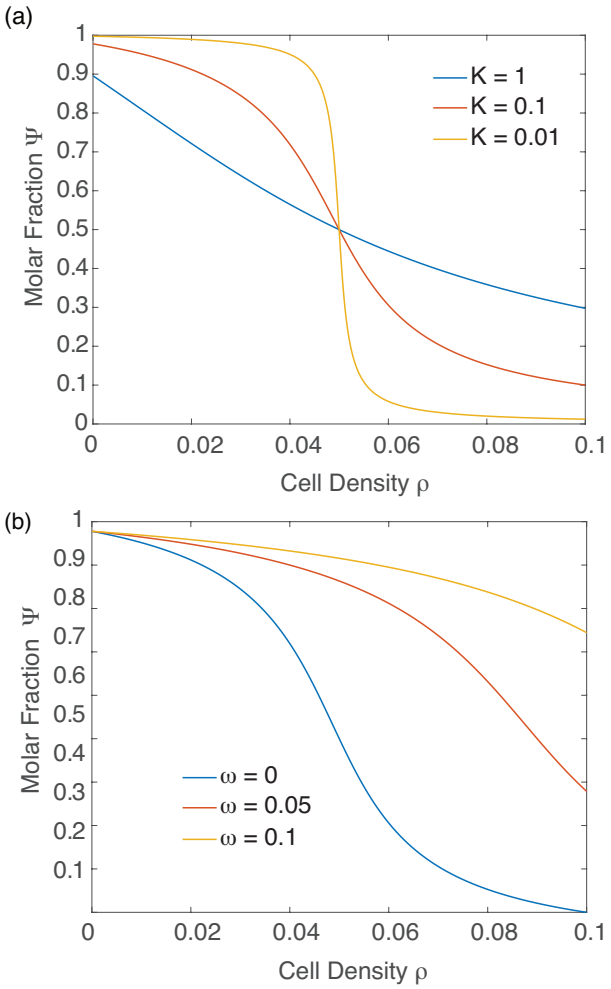



**Fig. 11** Dependence of response on population density for different values of mass-transfer. (a) LuxU-P response with zero mass-transfer, $\omega = 0$ and different levels of sensitivity, which is controlled by $K$ and $Q$ where we set $Q = K$. It is essentially a plot of (3.12) for different $K$ values. (b) For a fixed response sensitivity, $K = Q = 0.1$, equilibrium LuxU-P level increases as mass-transfer rate increases, so that the system acts as if it is in a low density environment. Other parameter values as Fig. 10.

ON (low levels of LuxU-P) when the cell density is sufficiently high and the mass transfer is sufficiently low. As we previously highlighted, this is the appropriate scenario when the target molecules of the QS system are secretory. Note that, as in the single-cell model, changing $K$ and $Q$ alters the sensitivity of the model. This is further illustrated in Fig. 11(a), which

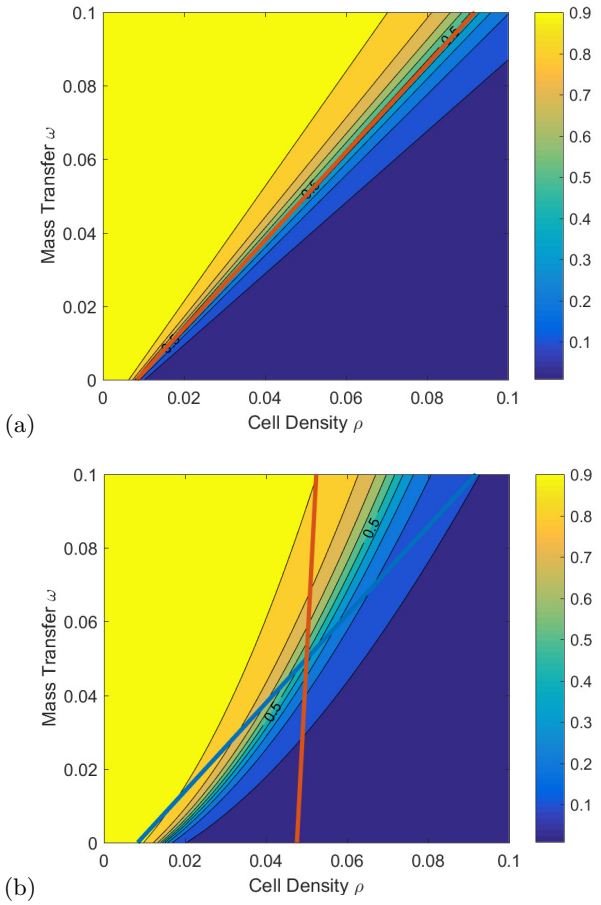



**Fig. 12** Reducing the effect of mass transfer on sensing cell density. Contour plots of $\Psi(\rho,\omega)$ as a function of $\rho,\omega$ for $K = 0.03$ and $Q = 0.025$ (high gain). Other parameters are the same as Fig. 3, except where stated. (a) Symmetric case with $\Gamma_2 = \Gamma_1 = 1.07$, $\gamma_2 = \gamma_1 = 0.01$ (slow decay), and $\kappa_2 = \kappa_1 = 30$. The red line indicates the contour $u_1 = u_2 = \theta$ for some fixed $\theta$. (b) Asymmetric case in which chemical properties of A2 are changed; $\Gamma_2 = 12.35$, $\gamma_2 = 1$ (fast decay), $\kappa_2 = 30$. The contours are now more vertical indicating a reduced sensitivity to mass transfer. There is now a separation of the contours $u_j = \theta$ for the durable signal $A1$ (blue line) and the fragile signal $A2$ (red line).

indicates how the population response varies with cell density in the case of zero mass transfer and different values of $K$ with $K = Q$.

Figs. 11(b) and Fig. 12(a) demonstrate that increasing the level of mass transfer ($\omega \neq 0$) increases the LuxU-P level, which switches the QS system OFF even when the population density is high. That is, the system acts as if it is in a low density environment. This is a problem when the downstream target of the QS system is gene expression of non-secretory molecules. Mathematically speaking, reducing the dependence on mass transfer and thus obtaining a more accurate estimate of cell density can be achieved by taking one or both of the autoinducers to have fast decay rates so that $\gamma_i \gg \omega$, see equation (4.5). However, this tends to reduce the selectivity of the QS system to high-density/low mass transfer environments. For the sake of illustration, suppose that A1 is durable (slow decay rate), whereas A2 is fragile (fast decay rate), following along analogous lines to [2,19]. The effects on the response are plotted in Fig. 12(b). It can be seen that the contours are more vertical, indicating a greter sensitivity to cell density.

## 5 Two-population model

Suppose that we partition the population of section 3 into two distinct bacterial populations, with cells of population 1 labeled by $j = 1, \ldots, N_1$ and cells of population 2 labeled by $l = 1, \ldots, N_2$ such that $N_1 + N_2 = N$. For the sake of illustration, we assume that the only difference between cells in the two populations is the rate of production of autoinducers $A_i$. An example is shown in Fig. 13, where each population produces its own distinct autoinducer. More generally, suppose that the production rate of $A_i$, $i = 1, \ldots, M$, is $\Gamma_i$ in population 1 and $\widetilde{\Gamma}_i$ in population 2. For a given $i$, let $(u_{ij}, r_{ij})$ denote the intracellular autoinducer concentration and bound receptor concentration in the $j$th cell of population 1, and similarly let $(v_{il}, s_{il})$ denote the corresponding quantities in the $l$th cell of population 2. The system of equations (3.1) become

$$\dot{r}_{ij} = k_{-i}(R_{Ti} - r_{ij}) - k_i r_{ij} u_{ij}, \quad j = 1, \ldots, N_1 \tag{5.1a}$$

$$\dot{u}_{ij} = \Gamma_i + k_{-i}(R_{Ti} - r_{ij}) - k_i r_{ij} u_{ij} - \kappa_i(u_{ij} - U_i), \tag{5.1b}$$

$$\dot{s}_{il} = k_{-i}(R_{Ti} - s_{ij}) - k_i s_{il} v_{il}, \quad l = 1, \ldots, N_2 \tag{5.1c}$$

$$\dot{v}_{il} = \widetilde{\Gamma}_i + k_{-i}(R_{Ti} - s_{il}) - k_i s_{il} v_{il} - \kappa_i(v_{il} - U_i), \tag{5.1d}$$

$$\dot{U}_i = \kappa_i(\rho_1 u_{av}^i + \rho_2 v_{av}^i - \rho U_i) - \gamma_i U_i, \tag{5.1e}$$

for $i = 1, \ldots, M$, with

$$u_{av}^i = \frac{1}{N_1}\sum_{j=1}^{N_1} u_{ij}, \quad v_{av}^i = \frac{1}{N_2}\sum_{l=1}^{N_2} v_{ij}, \tag{5.2}$$

and $\rho_k = N_k v_{cyt}/V_{ext}$, $k = 1, 2$.

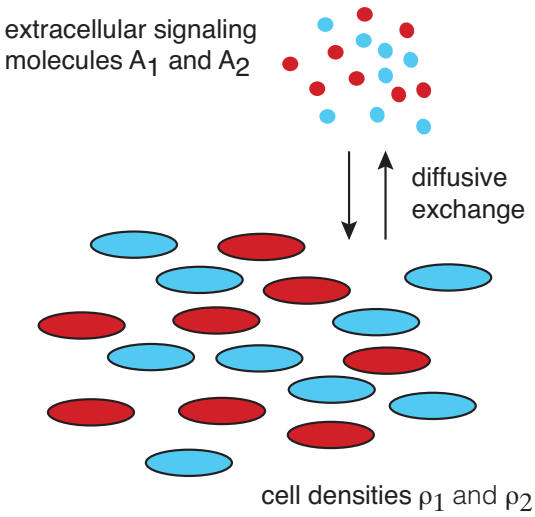



**Fig. 13** Two-population model with cell densities $\rho_j$ , $j = 1, 2$, producing and sensing two types of autoinducer $A_1$ and $A_2$, which are exchanged with the extracellular environment. Shown is the limiting case where population 1 produces $A_1$ and population 2 produces $A_2$. However, all cells detect both $A_1$ and $A_2$.

Following the analysis of the one population model, we can prove that the two-population model reduces to an effective single-cell model using the contraction theorem. First, we rewrite equations (5.1a-d) as the pair of vector-valued equations

$$\frac{d\mathbf{x}_j^i}{dt} = \mathbf{f}^i(\mathbf{x}_j^i, t) + \Gamma_i \begin{pmatrix} 1 \\ 0 \end{pmatrix}, \quad j = 1, \ldots, N_1 \tag{5.3a}$$

$$\frac{d\widetilde{\mathbf{x}}_l^i}{dt} = \mathbf{f}^i(\widetilde{\mathbf{x}}_l^i, t) + \widetilde{\Gamma}_i \begin{pmatrix} 1 \\ 0 \end{pmatrix}, \quad l = 1, \ldots, N_2 \tag{5.3b}$$

with $\mathbf{x}_j^i = (u_{ij}, r_{ij}) \in \mathbb{R}^2$, $(\mathbf{x}_j^i)_1 = u_{ij}$, and $\mathbf{f}^i$ given by equation (3.4). Although $\mathbf{x}_j^i$ and $\widetilde{\mathbf{x}}_j^i$ are coupled via equation (5.1e), for the purposes of contraction analysis, we can simply take $U_i(t)$ to be a common input, and treat equations (5.3a) and (5.3b) as independent. It follows that if the virtual systems

$$\frac{d\mathbf{y}}{dt} = \mathbf{f}^i(\mathbf{y}, t) + \Gamma_i \begin{pmatrix} 1 \\ 0 \end{pmatrix}, \tag{5.4a}$$

$$\frac{d\widetilde{\mathbf{y}}}{dt} = \mathbf{f}^i(\widetilde{\mathbf{y}}, t) + \widetilde{\Gamma}_i \begin{pmatrix} 1 \\ 0 \end{pmatrix} \tag{5.4b}$$

for $i = 1, \ldots, M$ are contracting with respect to $\mathbf{y}$ and $\widetilde{\mathbf{y}}$, respectively, then $(u_{ij}(t), r_{ij}(t)) \to (u_i(t), r_i(t))$ and $(v_{ij}(t), s_{ij}(t)) \to (v_i(t), s_i(t))$ in the large

time limit. We thus obtain the effective single-cell model

$$\dot{r}_i = k_{-i}(R_{Ti} - r_i) - k_i r_i u_i, \tag{5.5a}$$
$$\dot{u}_i = \Gamma_i + k_{-i}(R_{Ti} - r_i) - k_i r_i u_i - \kappa_i(u_i - U_i), \tag{5.5b}$$
$$\dot{s}_i = k_{-i}(R_{Ti} - s_i) - k_i s_i v_i, \tag{5.5c}$$
$$\dot{v}_i = \Gamma_i + k_{-i}(R_{Ti} - s_i) - k_i s_i v_i - \kappa_i(v_i - U_i), \tag{5.5d}$$
$$\dot{U}_i = \kappa_i(\rho_1 u_i + \rho_2 v_i - \rho U_i) - \gamma_i U_i \tag{5.5e}$$

for $i = 1, \ldots, N$. These equations have the unique stable fixed point $\mathbf{u} = \mathbf{u}^*$ and $\mathbf{v} = \mathbf{v}^*$ with

$$u_i^* = \frac{\rho_1 \Gamma_i + \rho_2 \widetilde{\Gamma}_i}{\gamma_i} + \frac{\Gamma_i}{\kappa_i} \equiv \psi_i(\rho_1, \rho_2), \tag{5.6a}$$
$$v_i^* = \frac{\rho_1 \Gamma_i + \rho_2 \widetilde{\Gamma}_i}{\gamma_i} + \frac{\widetilde{\Gamma}_i}{\kappa_i} \equiv \widetilde{\psi}_i(\rho_1, \rho_2). \tag{5.6b}$$

We can now determine the response of any cell in population 1 by setting $u_i = u_i^*$ in equation (2.14), which yields the following steady-state fractional concentration of LuxU-P is

$$\frac{[\text{LuxU-P}]_1}{[\text{LuxU-P}]_1 + [\text{LuxU}]_1} = \phi^{\text{eq}}\left(\boldsymbol{\psi}(\rho_1, \rho_2)\right) \equiv \Psi(\rho_1, \rho_2), \tag{5.7}$$

Similarly, for any cell in population 2,

$$\frac{[\text{LuxU-P}]_2}{[\text{LuxU-P}]_2 + [\text{LuxU}]_2} = \phi^{\text{eq}}\left(\widetilde{\boldsymbol{\psi}}(\rho_1, \rho_2)\right) \equiv \widetilde{\Psi}(\rho_1, \rho_2). \tag{5.8}$$

As a specific example, suppose that there are two autoinducers ($M = 2$) such that cells in population 1 produce $A_1$ and cells in population 2 produce $A_2$ along the lines of Fig. 13. In other words,

$$\Gamma_i = \Gamma \delta_{i,1}, \quad \widetilde{\Gamma}_i = \Gamma \delta_{i,2}.$$

We then have

$$\psi_i(\rho_1, \rho_2) = \Gamma\left(\frac{\rho_1 \delta_{i,1} + \rho_2 \delta_{i,2}}{\gamma_i} + \frac{\delta_{i,1}}{\kappa_i}\right), \tag{5.9a}$$
$$\widetilde{\psi}_i(\rho_1, \rho_2) = \Gamma\left(\frac{\rho_1 \delta_{i,1} + \rho_2 \delta_{i,2}}{\gamma_i} + \frac{\delta_{i,2}}{\kappa_i}\right). \tag{5.9b}$$

The two autoinducer concentrations $u_1, u_2$ thus act as proxies for the two cell densities $\rho_1, \rho_2$. In Fig. 14(a) we plot the resulting response function $\Psi(\rho_1, \rho_2)$ of population 1 as a function of the cell densities $\rho_1$ and $\rho_2$. (Identical curves would be obtained for population 2.) It can be seen that the QS system is only activated in regions where both cell densities are high. One could also consider more correlated production rates of the form

$$\Gamma_i = \Gamma \delta_{i,1} + \overline{\Gamma} \delta_{i,2}, \quad \widetilde{\Gamma}_i = \Gamma \delta_{i,2} + \overline{\Gamma} \delta_{i,1},$$

with $\Gamma \geq \overline{\Gamma}$, see Fig. 14(b). If $\Gamma = \overline{\Gamma}$ then the system response would only depend on the total density $\rho$.

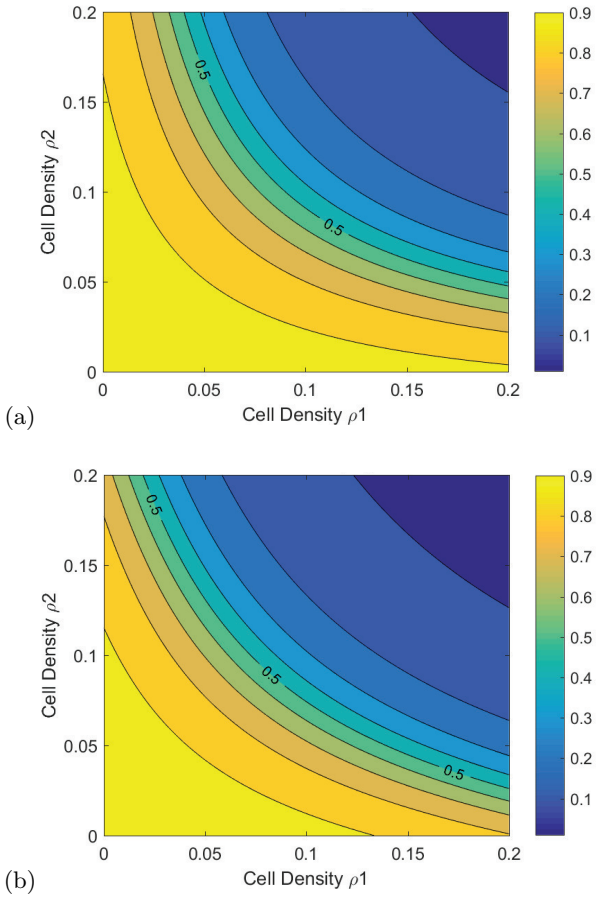



**Fig. 14** Contour plots of $\Psi(\rho_1, \rho_2)$ showing the $[\text{LuxU-P}]_1$ response of population 1 to changes in the densities of a two-population model. (a) $\Gamma_1 = 1$, $\Gamma_2 = 0$, $\widetilde{\Gamma}_1 = 0$, $\widetilde{\Gamma}_2 = 1$. (b) $\Gamma_1 = 1$, $\Gamma_2 = 0.1$, $\widetilde{\Gamma}_1 = 0.1$, $\widetilde{\Gamma}_2 = 1$. Other parameters used: $K = Q = 0.1$, $\gamma_1 = \gamma_2 = 0.1$, $\kappa_1 = \kappa_2 = 10$. The rest are the same as Fig. 3

## 6 Discussion

In this paper, we constructed a mathematical model of QS with multiple parallel input pathways. We first studied a single-cell model where one PdPC is driven by multiple signal inputs. Through fast-slow systems analysis, we determined the PdPC response as a function of input autoinducer concentrations. Further, we studied how different parameters, such as receptor numbers and reaction rates, affect the PdPC response. Next, we constructed a one population model and exploited the convergence properties of the population model to derive an effective single-cell model. Moreover, we considered two extensions of the population model in order to investi-

gate signal integration of more than one environmental variable, such as cell density and mass transfer, or two distinct cell densities.

One of the major simplifications of our model was to ignore the effects of feedback from downstream signaling pathways. It has been found experimentally that they are multiple feedback loops in the structure of QS in *V. harveyi* [25]. In future work, we would like to include those feedback loops in our model in order to quantify their roles in QS. Moreover, we would like to study how feedback loops may help the cell to counteract noise in the system. Finally, it has been found that quorum sensing expression changes at different developmental stages of a population [27]. This could be incorporated into our model by considering time-dependent population densities, for example.

## Acknowledgments

This work was supported by the National Science Foundation (DMS 1613048 and RTG 1148230)

## References

1. Bressloff, P. C. 2016. Ultrasensitivity and noise amplification in a model of V. harveyi quorum sensing. Physical Review E 93, 062418
2. Cornforth, D. M., Popat, R., McNally, L., Gurney, J., Scott-Phillips, D. M., Ivens, A., Diggle, S. P, Brown S. P. 2014 Combinatorial quorum sensing allows bacteria to resolve their social and physical environment. Proceedings of the National Academy of Sciences. 111, 4280-4284.
3. Davies, D. G., Parsek, M. R., Pearson, J. P., Iglewski, B. H. , Costerton, J. W., Greenberg, E. P. 1998. The involvement of cell-to-cell signals in the development of bacterial biofilm. Science 280 295-298
4. Dockery, J. D., Keener, J. P. 2001. A mathematical model for quorum-sensing in Pseudomonas aeruginosa. Bull. Math. Biol. 63, 95-116.
5. Dunlap, P. V. 1999 Quorum regulation of luminescence in Vibrio fischeri. J. Mol. Microbiol. Biotechnol. 1, 5-12
6. Fuqua, C., Winans, S. C., Greenberg, E. P. 1996. Census and consensus in bacterial ecosystems: the LuxR-LuxI family of quorum-sensing transcriptional regulators. Annu. Rev. Microbiol. 50 727-751
7. Ge, H., Qian, M. 2008. Sensitivity amplification in the phosphorylation-dephosphorylation cycle: nonequilibrium steady states, chemical master equation and temporal cooperativity. J. Chem. Phys. 129 015104.
8. Goldbeter A, Koshland DE. 1981. An amplified sensitivity arising from covalent modification in biological systems. Proc. Natl. Acad. Sci. USA 78:684-6844
9. Goryachev, A. B. 2009. Design principles of the bacterial quorum sensing gene networks. WIRE Syst. Biol. Med. 1, 45-60.
10. Hense, B. A., Kuttler, C., Muller, J., Rothballer, M., Hartmann, A., Kreft, J-U. 2007 Does efficiency sensing unify diffusion and quorum sensing? Nat. Rev. Microbiol. 5, 230-239.

11. Hunter, G. A. M., Guevara Vasquez, F., Keener, J. P. 2013. A mathematical model and quantitative comparison of the small RNA circuit in the *Vibrio harveyi* and *Vibrio cholerae* quorum sensing systems. Phys. Biol. 10 046007.
12. Jung, S. A., Hawver, L. A., Ng, W. L. 2016. Parallel quorum sensing signaling pathways in *Vibrio cholerae* Curr. Genet. 62 255
13. Lenz, D. D H., Mok, K. C., Lilley, B. N., Kulkarni, R. V., 2004. Wingreen, N. S., Bassler, B. L.. The small RNA chaperone Hfq and multiple small RNAs control quorum sensing in *Vibrio harveyi* and *Vibrio cholerae*. Cell 118 69-82.
14. Long, T., Tu, K. C. , Wang, Y., Mehta, P., Ong, N.P., Bassler, B. L., Wingreen, N. S. 2009. Quantifying the integration of Quorum-Sensing Signal with Single-Cell Resolution. PLoS Biol 7(3): e1000068.
15. Mehta, P., Goyal, S., Long, T., Bassler, B. L., Wingreen, N. 2009. Information processing and signal integration in bacterial quorum sensing. Mol. Syst. Cell Biol. 5 (325), 1-11
16. Miyashiro, T., Ruby, E. G. 2012. Shedding light on bioluminescence regulation in Vibrio fischeri. Mol.Microbiol. 84, 795-806
17. Ng, W. L, Bassler, B. L. 2009. Bacterial quorum-sensing network architectures. Annu. Rev. Genet. 43, 197-222
18. Papenfort, K., Bassler, B. L. 2016. Quorum sensing signal-response systems in Gram-negative bacteria. Nat. Rev. Microbiol.14, 577-588.
19. Popat, R, Cornforth, D. M., McNally, L., Brown, S. P. 2015 Collective sensing and collective responses in quorum-sensing bacteria. J. R. Soc. Interface 12: 20140882.
20. Qian, H. 2012. Cooperativity in cellular biochemical processes. Annu. Rev. Biophys. 41, 179-204.
21. Redfield R. J. 2002 Is quorum sensing a side effect of diffusion sensing? Trends Microbiol. 10, 365-370.
22. Russo, G., Slotine, J. J. E. 2010 Global convergence of quorum sensing network. Phys. Rev. E 82, 041919
23. Lohmiller, W., Slotine, J. J. E. 1998. On contraction analysis of nonlinear systems. Automatica 34, 683-696.
24. Swem, L. R., Swem, D. L., Wingreen, N. S., Bassler, B. L. 2008. Deducing receptor signaling parameters from in vivo analysis: LuxN/AI-1 quorum sensing in *Vibrio harveyi* Cell 134 461-473
25. Teng, S.-W., Schaffer, J. N., Tu, K. C., Mehta, P., Lu, W., Ong, N. P., Bassler, B. L., Wingreen, N. S. 2011. Active regulation of receptor ratios controls integration of quorum-sensing signals in *Vibrio harveyi*. Molecular Systems Biology, 7, 491.
26. Waters, C. M., Basser, B. L. 2005. Quorum sensing: Cell-to-cell communication in bacteria. Annu. Rev. Cell Dev. Biol. 21, 319-346
27. Waters, C. M., Basser, B. L. 2006. The *Vibrio harveyi* quorum-sensing system uses shared regulatory components to discriminate between multiple autoindcucer. Genes & Development, 20(19), 2754–2767.
28. Wei, Y,. Ng, W.-L., Cong, J. Bassler, B. L. 2012. Ligand and antagonist driven regulation of the *Vibrio cholerae* quorum-sensing receptor CqsS. Mol. Microbiol. 83 1095-1108.
29. West S. A., Winzer, K., Gardner, A., Diggle, S. P. 2012 Quorum sensing and the confusion about diffusion. Trends Microbiol. 20, 586-594.